JGR Space Physics

RESEARCH ARTICLE
10.1029/2020JA028012

Wave Normal Angle Distribution of Magnetosonic Waves in the Earth's Magnetosphere: 2-D PIC Simulation

Jicheng Sun[1], **Lunjin Chen**[2], **and Xueyi Wang**[1]

[1]Department of Physics, Auburn University, Auburn, AL, USA, [2]Department of Physics, University of Texas at Dallas, Richardson, TX, USA

Key Points:
- Using 2-D PIC simulations, the wave normal angle distribution of magnetosonic waves has been investigated
- The wave normal angles are distributed over a narrow range (82°–89°) during the linear growth stage
- The wave normal angles decrease with the increase of the ring velocity of the proton ring distribution

Correspondence to:
J. Sun,
jzs0215@auburn.edu

Citation:
Sun, J., Chen, L., & Wang, X. (2020). Wave normal angle distribution of magnetosonic waves in the Earth's magnetosphere: 2-D PIC simulation. *Journal of Geophysical Research: Space Physics*, *125*, e2020JA028012. https://doi.org/10.1029/2020JA028012

Received 13 MAR 2020
Accepted 21 APR 2020
Accepted article online 5 MAY 2020

Abstract Radiation belt electrons can be accelerated and scattered by magnetosonic waves in the Earth's magnetosphere, and the scattering rate of electrons is sensitive to the wave normal angle. However, observationally it is difficult to identify the wave normal angle within a few degrees. In this study, using 2-D particle-in-cell (PIC) simulations, we investigate the wave normal angle distribution of magnetosonic waves excited by ring distribution protons. Both the linear theory and simulations have shown that the wave normal angles are distributed over a narrow range (82°–89°) with a major peak at about 85° during the linear growth stage when the proton ring velocity is close to the Alfven speed. In addition, 2-D PIC simulations further demonstrated that the waves tend to have larger wave normal angles (84°–89°) during the saturation stage since the waves with smaller wave normal angles are dissipated faster. It is also found that wave normal angles decrease with the increase of wave frequency. With the increase of the ring velocity of the proton ring distribution, the perpendicular wavenumber of excited magnetosonic waves decreases, which leads to the decrease of the wave normal angle. The simulation results provide a valuable insight to understand the property of magnetosonic waves, and the findings are useful for the global simulations of radiation belt dynamics.

1. Introduction

Equatorial magnetosonic waves are an electromagnetic emission naturally occurring in the Earth's magnetosphere (Gurnett, 1976; Russell et al., 1970; Santolík et al., 2002; Tsurutani et al., 2014). These waves propagate nearly perpendicularly to the background magnetic field. Observationally it has been shown that the waves typically exhibit a series of harmonics of the proton gyrofrequency up to the lower hybrid frequency (e.g., Balikhin et al., 2015). Recent studies also reported some new complicated features such as rising-tone spectra and quasi-periodicity in time (Boardsen et al., 2014; Fu et al., 2014). Magnetosonic waves in the inner magnetosphere are also known as equatorial noise since they are usually observed within a few degrees of the geomagnetic equator (Ma et al., 2013; Russell et al., 1970). The statistical study has shown that magnetosonic waves can occur both inside and outside the plasmasphere, with a preferential occurrence at the dusk sector (Yuan et al., 2019). Satellite observations show a link between the excitation of magnetosonic waves and proton ring distribution at energies about dozens of keV (Boardsen et al., 1992; Meredith et al., 2008; Perraut et al., 1982). Then, both linear theory (Chen et al., 2010; Min & Liu, 2016; Sun, Gao, Chen, et al., 2016) and PIC simulations (Liu et al., 2011; Sun, Gao, Lu, et al., 2016) have demonstrated that the waves can be generated by a ring distribution of protons with the positive phase space density gradient around the local Alfven speed.

In recent years, there has been an increasing interest in magnetosonic waves due to their potential roles in both accelerating and scattering radiation belt electrons (Horne et al., 2007; Horne & Thorne, 1998; Li et al., 2014; Ni et al., 2017; Xiao et al., 2015). Horne et al. (2007) suggested that magnetosonic waves can accelerate radiation belt electrons through Landau resonance, and the corresponding timescale can be as short as 1 day. This time scale is comparable to that of acceleration due to cyclotron resonance with whistler mode chorus (Horne et al., 2005), suggesting the importance of magnetosonic waves in radiation belt electron acceleration. Since Landau resonant scattering of electrons relies on the parallel wavenumber, which is sensitive to the exact value of the wave normal angle θ near 90°, the scattering rate is sensitive to the wave normal angle. Magnetosonic waves can also interact with radiation belt electrons via bounce resonance (Chen et al., 2015; Tao & Li, 2016). Using a test particle simulation, Chen et al. (2015) demonstrated that the effect of bounce resonance of magnetosonic waves on equatorially mirroring electrons is also sensitive to the wave normal angle. It is interesting to note that transit time scattering of energetic electrons can

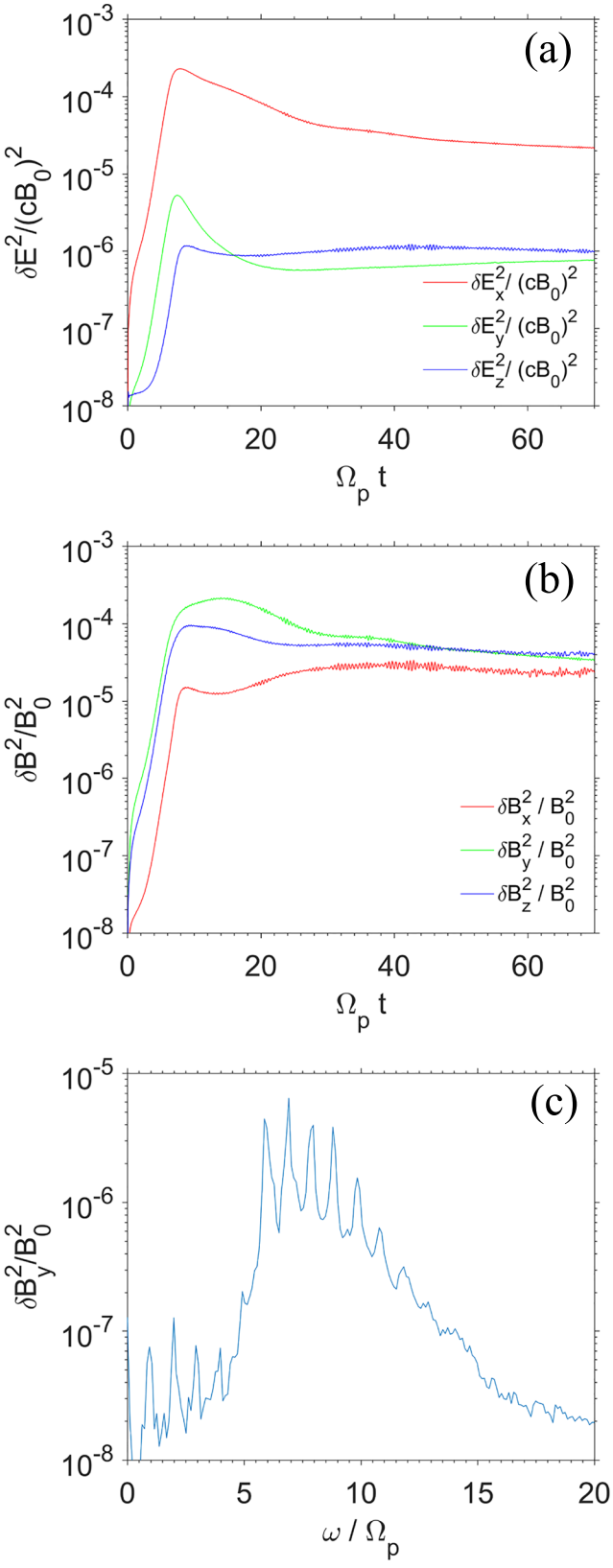

Figure 1. The time evolution of spatially averaged fluctuating (a) electric fields and (b) magnetic fields, and (c) the power spectrum of fluctuating magnetic field δB_y for Case 1.

occur due to spatial confinement of magnetosonic waves near the equator (Bortnik et al., 2015; Bortnik & Thorne, 2010). In addition to interacting with energetic electrons, PIC simulations revealed that magnetosonic waves can result in the energization of background thermal electrons and protons (Chen et al., 2018; Sun et al., 2017). These findings were later confirmed by the satellite observations (Yuan et al., 2018).

Both quasi-linear theory (Mourenas et al., 2013; Li et al., 2014) and test particle simulation (Chen et al., 2015; Lei et al., 2017) have shown that the scattering rate of electrons is sensitive to the wave normal angle of magnetosonic waves. Compared to the waves with $\theta = 89.5°$, the magnetosonic waves with $\theta = 87°$ have a much stronger efficiency to scatter the near 90° pitch angle electrons (Lei et al., 2017). Thus, the exact value of the wave normal angle is an important parameter to model the effect of magnetosonic waves on the radiation belt electron dynamics. However, observationally it is difficult to identify the wave normal angle within a few degrees (Yuan et al., 2019; Zou et al., 2019). In this study, using the linear theory and PIC simulations, we investigate the wave normal angle characteristics of magnetosonic waves excited by ring distribution protons. The structure of this paper is as follows. Section 2 describes the PIC simulation model and initial parameters. Then, the simulation results are presented in section 3. At last, conclusions and discussion are given in section 4.

2. Simulation Model

The PIC simulation provides a powerful tool to study the waves in the space plasma (e.g., Chen et al., 2016; Sun et al., 2019). In this paper, 2-D electromagnetic PIC simulations are employed to investigate the wave normal angle distribution of magnetosonic waves driven by a proton ring distribution. The simulation domain lies in the x-y plane and the background magnetic field $\mathbf{B_0}$ is along the y-axis. Periodic boundary conditions are used in both dimensions. The simulation model consists of three plasma components: cool electrons, cool protons, and ring distribution protons. Their number densities are n_e, n_{pc}, and n_{pr}, respectively, and satisfy the condition $n_e = n_{pc}+n_{pr}$ for the sake of charge neutrality. The cool electrons and cool protons are assumed to satisfy a Maxwellian distribution. The distribution of ring distribution protons is given by $f_{pr} = n_{pr}\delta(v_{\parallel})\delta(v_{\perp} - V_R)/(2\pi v_{\perp})$, where $v_{\parallel}$ and $v_{\perp}$ are velocities parallel and perpendicular to the background magnetic field, and V_R is the proton ring velocity. Hereafter, subscripts e, pc, and pr represent cool electrons, cool protons, and ring distribution protons, respectively.

In our simulations, the magnetic field is normalized to B_0, and the number density is expressed in the units of the cool electron density n_e. The time and space are normalized to the inverse of proton gyrofrequency $\Omega_p = eB_0/m_p$ and the proton inertial length $\lambda_i = \sqrt{m_p/n_e\mu_0 e^2}$, respectively, where m_p is the proton mass, e is the elementary charge, and μ_0 is the vacuum permeability. Due to the nearly perpendicular propagation of the magnetosonic waves, we choose spatial domain in the simulation to have spatial length perpendicular to the background magnetic field $L_x = 10\pi\lambda_i$ (with corresponding grid number $N_x = 1{,}024$) and spatial length parallel to the background magnetic field $L_y = 50\pi\lambda_i$ (with corresponding grid number $N_y = 512$). There are on average 200 macroparticles in each of the $N_x \times N_y$ cells for each of the three species. Here a smaller light speed $c/V_A = 20$ is chosen to improve the computational efficiency,

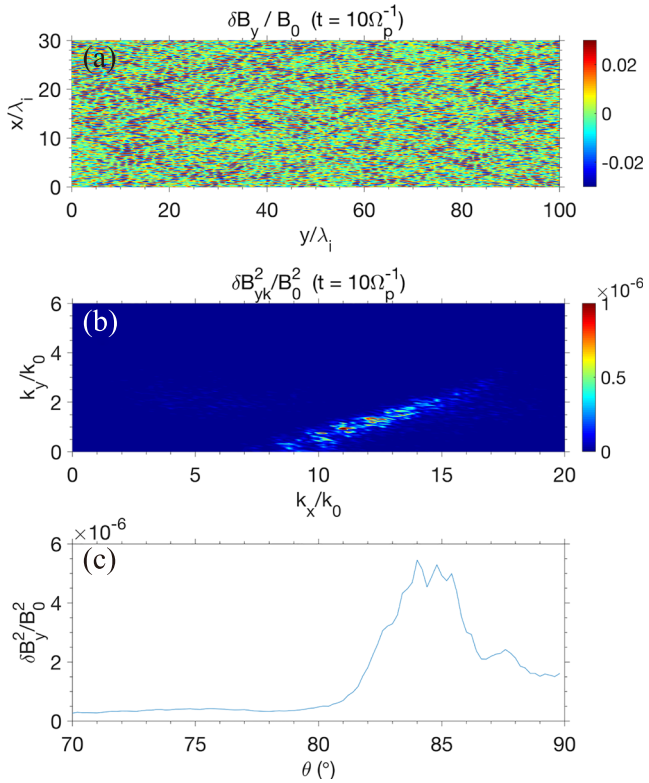

Figure 2. (a) The contour plot and (b) the wavenumber power spectrum of fluctuating magnetic field δB_y, and (c) the wave normal angle distribution at $\Omega_p t = 10$ for Case 1.

where V_A is the Alfven speed. Then, the ion plasma frequency to gyrofrequency ratio ω_p/Ω_p is 20 in the simulations. A reduced proton-to-electron mass ratio $m_p/m_e = 100$ is adopted for the same reason. Our previous theoretical and simulation studies (Sun, Gao, Chen, et al., 2016; Sun, Gao, Lu, et al., 2016) have investigated the effects of the mass ratio and the speed of light on the wave spectrum. The smaller mass ratio and the smaller light speed than the actual value may reduce the low hybrid frequency of the system and cause changes in the frequency of magnetosonic waves compared to the proton cyclotron frequency. The time step is $\Delta t = 5 \times 10^{-4}$ Ω_p^{-1} such that electron dynamics can be fully resolved. Initially, the thermal speed of the cool protons is set to $0.0114V_A$ with the corresponding $\beta_p = 1.3 \times 10^{-4}$. The cool electrons adopt the same temperature as cool protons. The number density of ring distribution protons n_{pr}/n_e is 0.05.

3. Simulation Results

With the 2-D PIC simulation model and the simulation setup described above, we examine the wave normal angle distribution of magnetosonic waves excited by ring distribution protons. We will consider two cases with different proton ring velocities, $V_R/V_A = 1$ (Case 1) and $V_R/V_A = 2$ (Case 2), respectively.

Figures 1a and 1b show the time evolution of spatially averaged fluctuating electromagnetic fields for Case 1. It is clear that the waves begin to be excited from the very beginning and then undergo a linear growth stage before a saturation stage is reached at about $\Omega_p t = 20$. The saturated waves have dominant perpendicular electric field component δE_x and field-aligned magnetic component δB_y, indicating that the waves possess compressional magnetic field. This is consistent with the polarization of magnetosonic waves predicted by the linear theory (Gary et al., 2010). Figure 1c displays the power spectrum of fluctuating magnetic field which is obtained by Fourier transforming of $\delta B_y/B_0$ from $\Omega_p t = 0$ to 60. The power spectral density shows discrete peaks at harmonic frequencies from 6 to $11\Omega_p$.

To investigate the wave normal angle distribution of magnetosonic waves, we select for detailed diagnosis two representative moments: $\Omega_p t = 10$ at the linear growth stage and $\Omega_p t = 35$ at the nonlinear evolution stage. Figures 2a and 2b show the contour plot and the wavenumber power spectrum of fluctuating magnetic field δB_y at $\Omega_p t = 10$, respectively. In this paper, δB_{yk} represents the fluctuating magnetic field δB_y in the wavenumber space. From the contour plot of δB_y, we can see that the waves propagate mainly along the perpendicular (x) direction. It can be seen more clearly from Figure 2b that the dominant waves are mainly distributed in $10k_0 < k_x < 15k_0$ and $0.5k_0 < k_y < 2k_0$, where k_x and k_y are wavenumbers in x and y directions and k_0 is equal to λ_i^{-1}. The magnitude of perpendicular wavenumber k_x is consistent with the results of the previous 1-D PIC simulation (Sun, Gao, Lu, et al., 2016). The perpendicular wavenumber is much larger than the parallel wavenumber, which also indicates that the waves propagate almost perpendicularly to the background magnetic field. Note that the wave normal angle of magnetosonic waves becomes smaller as the wavenumber increases. Summing the power of magnetosonic waves along a given angle in wavenumber space, we can examine their wave normal angle distribution at $\Omega_p t = 10$ shown in Figure 2c. The wave normal angles of magnetosonic waves are mainly distributed between 82° and 89°.

To certify the wave normal angle distribution of magnetosonic waves obtained by the PIC simulation in the linear growth stage, we calculate the linear growth rate of the magnetosonic waves based on the initial simulation parameters. The linear theory model we use here is the same as Chen et al. (2015). Figure 3a displays the growth rate γ as a function of k_x and k_y. The modes with dominant growth rates ($\gamma > 0.4\Omega_p$) are mainly distributed around $10k_0 < k_x < 20k_0$ and $0.5k_0 < k_y < 3k_0$. This wavenumber regime is consistent with that for the simulated wave power spectrum (Figure 2b). Figure 3b shows the growth rate γ as a function of wave frequency ω, and the color in the figure indicates the wave normal angle of the waves. The frequency of

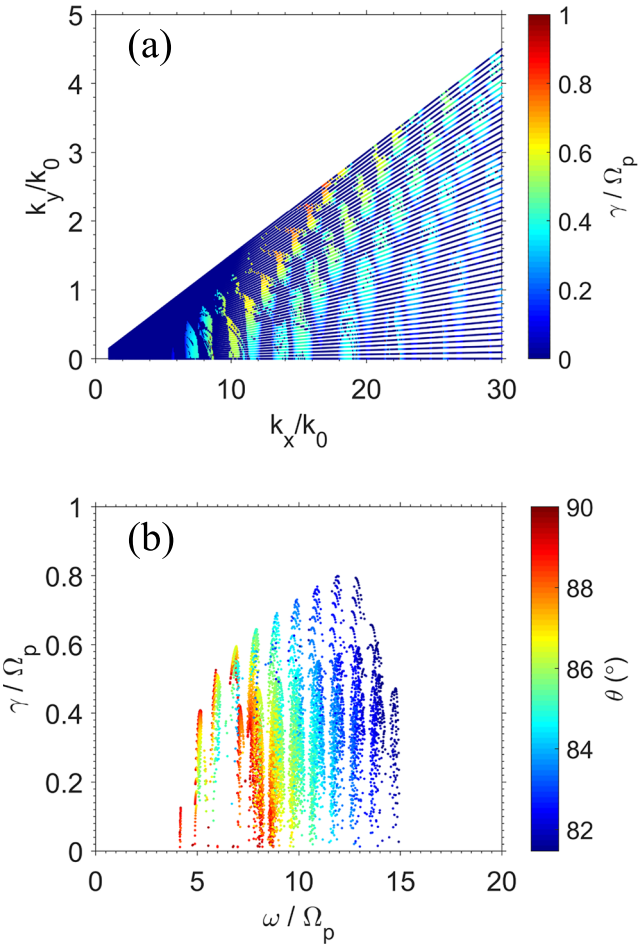

Figure 3. (a) The linear growth rate γ of magnetosonic waves as a function of k_x and k_y. (b) The linear growth rate γ versus the wave frequency ω and the color denotes the wave normal angle of the waves.

unstable modes obtained by the linear theory is mainly distributed between 5 and 15 Ω_p. The growth rate profile is mainly consistent with the spectral peaks obtained from the simulation (Figure 1c). The wave normal angles of the waves with frequencies of 5 to 10 Ω_p are above 85°, and the wave normal angles of the waves with frequencies of 11 to 15 Ω_p are located between 80° and 85°. Higher frequency magnetosonic waves have smaller wave normal angles, and these waves tend to dissipate quickly. The excited magnetosonic wave frequency in the simulation which includes the nonlinear evolution of the waves is smaller than the frequency predicted by the linear theory. Thus, it is safe to conclude that the fluctuating electromagnetic fields in our simulations are indeed magnetosonic waves generated by the ring distribution protons.

Figures 4a and 4b show the contour plot and the wavenumber power spectrum of fluctuating magnetic field δB_y at $\Omega_p t = 35$, respectively. The wave normal angle distribution of magnetosonic waves at this time is displayed in Figure 4c. As shown in Figure 4b, the power spectrum of magnetosonic waves has become very narrow in the wavenumber regime, in comparison with Figure 2b. During the nonlinear evolution stage, the wave normal angles of magnetosonic waves are approximately 84° to 89° (Figure 4c). Thus, compared to the linear growth stage, the magnetosonic waves in the nonlinear stage will be distributed over larger wave normal angles.

We also investigate the influence of the ring velocity of the proton ring distribution. Figure 5 displays the simulation results of Case 2 with the proton ring velocity V_R/V_A set to 2. We select two representative moments for detailed diagnosis, one at $\Omega_p t = 15$ for the linear growth stage and the other at $\Omega_p t = 35$ for the nonlinear evolution stage. Figures 5a and 5b illustrate the contour plot and the wavenumber power spectrum of fluctuating magnetic field δB_y at $\Omega_p t = 15$, respectively, while Figure 5c displays the wave normal angle distribution of magnetosonic waves at this time. Figures 5d–5f show the results at $\Omega_p t = 35$ using the same format as Figures 5a–5c. Compared with the results of Case 1 (Figure 2), we find from Figure 5b that with the increase of the proton ring velocity, the perpendicular wavenumber of magnetosonic waves becomes smaller, while the parallel wavenumber is almost the same. This leads to a smaller wave normal angle of the waves for Case 2, and the wave normal angle can be as small as about 75° (Figure 5c). The dependence of the wave normal angle and the ring velocity obtained by the simulation is consistent with that predicted from the linear theory (Min & Liu, 2016). In addition, similar to the result of Case 1, the wave normal angles in the nonlinear stage (Figure 5f) become larger than that in the linear growth stage (Figure 5c).

To further study the wave normal angle distribution of magnetosonic waves in the Earth's magnetosphere, we perform another 2-D simulation in the dipole magnetic field instead of the uniform magnetic field used above. The simulation setup is the same as that of Chen et al. (2018). This simulation model investigates the excitation of magnetosonic waves in the meridian plane, and the ring distribution protons are placed at the center of the simulation domain as the energy source of the waves. The plasma parameters of the source region in the model are consistent with those in Case 1 in this paper. Figure 6a shows the power spectral density of $\delta B_{\parallel}/B_0$ at the central location of the simulation region, and Figure 6b shows the wave normal angle θ of wave amplitude $\delta B_{\parallel}^2/B_0^2 > 5 \times 10^{-6}$. The wave normal angles are estimated by the algorithm in Means (1972). As shown in the figure, the wave normal angles are distributed between 80° to 90°. At 20 Ω_p^{-1} after reaching the maximum wave power, the energy of magnetosonic waves at lower frequency (5 Ω_p) is reduced to about 50% of its corresponding maximum value, while the energy at higher frequency (8 Ω_p) is reduced to about 10% of its corresponding maximum value. Therefore, the higher frequency waves tend to dissipate faster. These features are basically consistent with the results of Case 1. The nonlinear

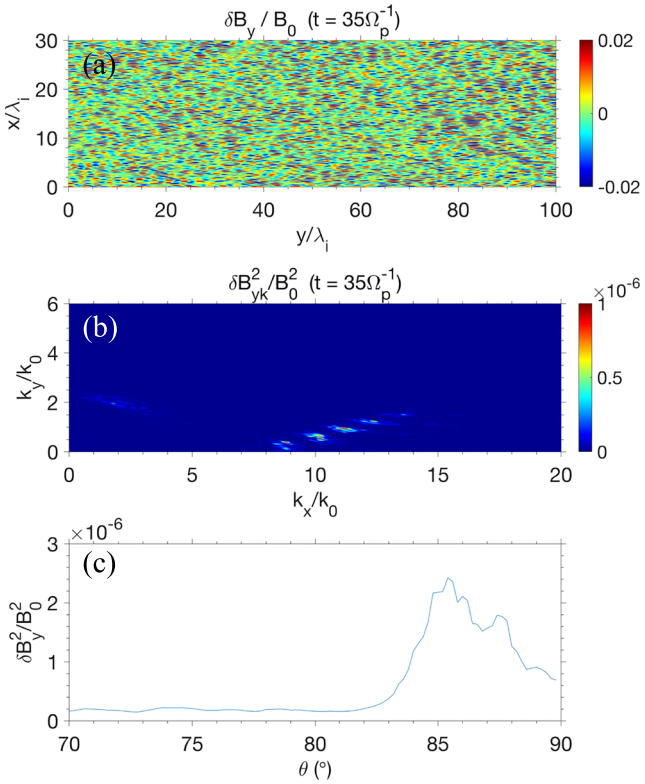

Figure 4. (a) The contour plot and (b) the wavenumber power spectrum of fluctuating magnetic field δB_y, and (c) the wave normal angle distribution at $\Omega_p t = 35$ for Case 1.

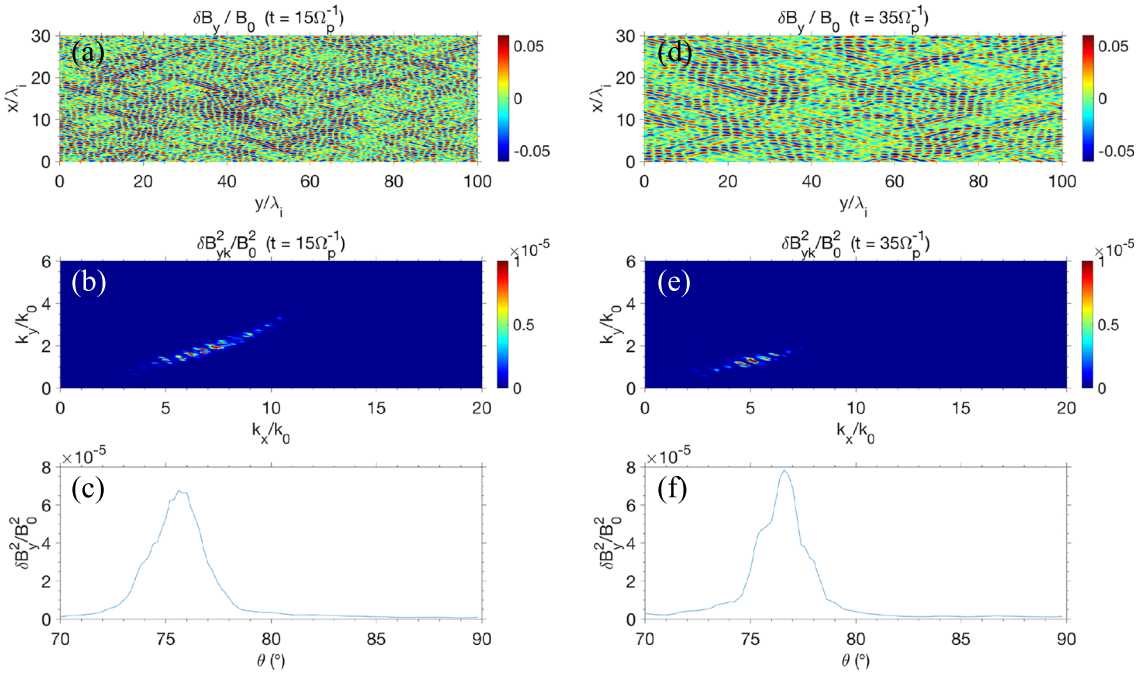

Figure 5. The contour plot of fluctuating magnetic field δB_y for Case 2 at (a) $\Omega_p t = 15$. (d) $\Omega_p t = 35$, (b) and (e) for the wavenumber power spectrum; and (c) and (f) for the wave normal angle distribution.

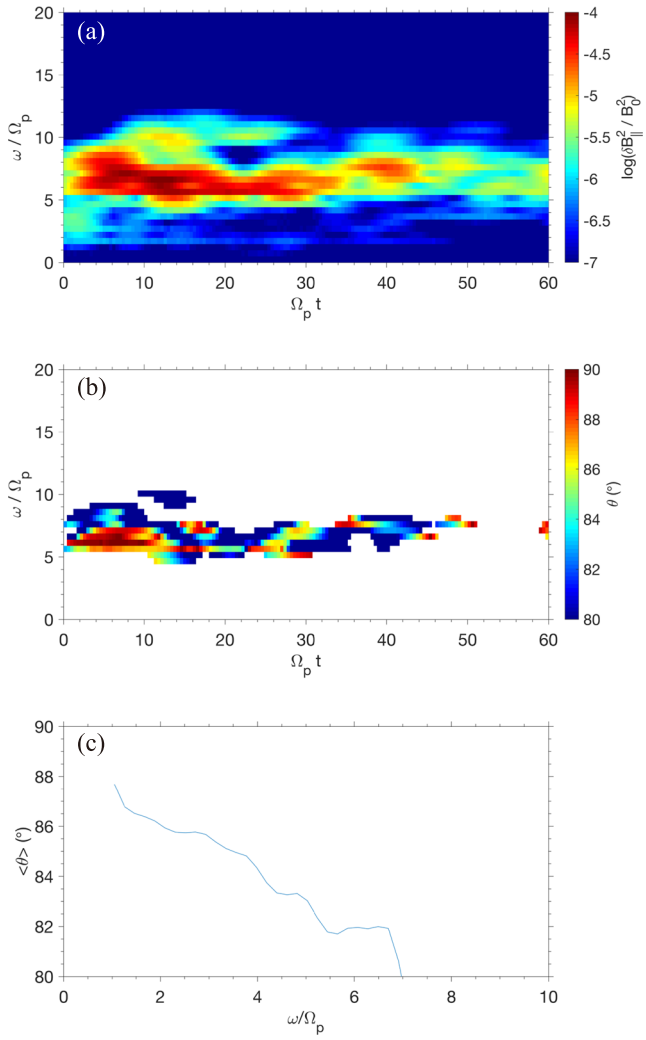

Figure 6. (a) The power spectral density of $\delta B_{\parallel}/B_0$ and (b) the wave normal angle as a function of frequency and time for the simulation in the dipole magnetic field. (c) The average wave normal angle $<\theta>$ versus the wave frequency ω.

evolution of electromagnetic waves in the simulation is complicated by wave propagation. The absorbing boundary conditions for electromagnetic fields used in the dipole field allow the excited waves to propagate out of the simulation region and leave the simulation system, while the periodic boundary conditions used in the uniform field will permit those waves reaching the boundary reenter the system. The former simulation tends to have smaller wave normal angle values than the uniform simulation. Therefore, the boundary condition may lead to the difference in the evolution of the wave normal angle distribution between the dipole field and the uniform field. Figure 6c displays the average wave normal angle weighted by wave intensity from $\Omega_p t = 0$ to 60 as a function of wave frequency ω for this simulation. The average wave normal angle for each frequency is calculated by $< \theta > = \sum_t \theta(t)\delta B_{\parallel}^2(t)/\sum_t \delta B_{\parallel}^2(t)$. The average wave normal angle decreases as the wave frequency increases, which is consistent with the result in the uniform field. These results support that the wave normal angle distribution obtained in the uniform magnetic field can be applied to the Earth's magnetosphere.

4. Conclusions and Discussion

In this paper, by performing 2-D PIC simulations, we have investigated the wave normal angle distribution of magnetosonic waves excited by ring distribution protons. Our study found that the wave normal angles are distributed over a narrow range (82°–89°) with a major peak at about 85° during the linear growth stage when the proton ring velocity V_R is close to V_A. In addition, 2-D PIC simulations further demonstrated that

the waves tend to have larger wave normal angles (84°–89°) during the saturation stage since the waves with smaller wave normal angles dissipate more quickly. It is also found that the wave normal angles decrease with the increase of wave frequency. With the increase of the ring velocity of the proton ring distribution, the perpendicular wavenumber of excited magnetosonic waves decreases, which leads to the decrease of the wave normal angle. The PIC simulation in the dipole magnetic field further demonstrates that the wave normal angle distribution obtained in the uniform magnetic field can be applied to the Earth's magnetosphere.

Radiation belt electrons can be accelerated and scattered by magnetosonic waves in the Earth's magnetosphere, and the scattering rate of electrons is sensitive to the wave normal angle. In previous studies (e.g., Bortnik & Thorne, 2010; Li et al., 2014; Ni et al., 2017), an assumed Gaussian wave normal angle distribution with a central peak at 89° or 89.5° is adopted, but there lacks justification for the central peak values. Our results indicate that the wave normal angle of the magnetosonic waves is smaller than the angles commonly used in the previous model. Thus, the scattering effect of the magnetosonic waves on the radiation belt electrons may be underestimated in the previous model. Limited by the computational resources, a reduced mass ratio and a smaller light speed are used in our simulations. Using the linear theory, it is shown that the increase of the mass ratio or the light speed tends to result in a slightly larger wave normal angle but does not change the essential physics. The wave normal angle is still significantly less than 89°. According to Mourenas et al. (2013), the wave normal angle smaller than 89° will lead to a more efficient pitch angle and momentum diffusion of relativistic electrons by magnetosonic waves, potentially even more efficient than scattering by chorus waves. In addition, the wave normal angle of magnetosonic waves is smaller in the linear stage than in the nonlinear evolution stage, which may affect the scattering rate of electrons in the radiation belt. It is interesting to note that the ring distribution protons can also generate the electromagnetic ion cyclotron waves (Min & Liu, 2016). The interaction between these waves excited self-consistently and radiation belt electrons in the dipole magnetic field will be investigated in the future.

Acknowledgments
We acknowledge the support from the NASA grant NNX17AI52G and the NSF grant 1702805 through the Geospace Environment Modeling program. The data supporting the conclusions in this paper have been available in OSF repository in the United States with http://10.17605/OSF.IO/BP5UH. We also thank Kaijun Liu and Quanming Lu for helpful discussions.

References

Balikhin, M. A., Shprits, Y. Y., Walker, S. N., Chen, L., Cornilleau-Wehrlin, N., Dandouras, I., et al. (2015). Observations of discrete harmonics emerging from equatorial noise. *Nature Communications*, *6*, 7703. https://doi.org/10.1038/ncomms8703

Boardsen, S. A., Gallagher, D. L., Gurnett, D. A., Peterson, W. K., & Green, J. L. (1992). Funnel-shaped, low-frequency equatorial waves. *Journal of Geophysical Research*, *97*, 14,967–14,976. https://doi.org/10.1029/92JA00827

Boardsen, S. A., Hospodarsky, G. B., Kletzing, C. A., Pfaff, R. F., Kurth, W. S., Wygant, J. R., & MacDonald, E. A. (2014). Van Allen probe observations of periodic rising frequencies of the fast magnetosonic mode. *Geophysical Research Letters*, *41*, 8161–8168. https://doi.org/10.1002/2014GL062020

Bortnik, J., & Thorne, R. M. (2010). Transit time scattering of energetic electrons due to equatorially confined magnetosonic waves. *Journal of Geophysical Research*, *115*, A07213. https://doi.org/10.1029/2010JA015283

Bortnik, J., Thorne, R. M., Ni, B., & Li, J. (2015). Analytical approximation of transit time scattering due to magnetosonic waves. *Geophysical Research Letters*, *42*, 1318–1325. https://doi.org/10.1002/2014GL062710

Chen, L., Maldonado, A., Bortnik, J., Thorne, R. M., Li, J., Dai, L., & Zhan, X. (2015). Nonlinear bounce resonances between magnetosonic waves and equatorially mirroring electrons. *Journal of Geophysical Research: Space Physics*, *120*, 6514–6527. https://doi.org/10.1002/2015JA021174

Chen, L., Sun, J., Lu, Q., Gao, X., Xia, Z., & Zhima, Z. (2016). Generation of magnetosonic waves over a continuous spectrum. *Journal of Geophysical Research: Space Physics*, *121*, 1137–1147. https://doi.org/10.1002/2015JA022089

Chen, L., Sun, J., Lu, Q., Wang, X., Gao, X., Wang, D., & Wang, S. (2018). Two-dimensional particle-in-cell simulation of magnetosonic wave excitation in a dipole magnetic field. *Geophysical Research Letters*, *45*, 8712–8720. https://doi.org/10.1029/2018GL079067

Chen, L., Thorne, R. M., Jordanova, V. K., & Horne, R. B. (2010). Global simulation of magnetosonic wave instability in the storm time magnetosphere. *Journal of Geophysical Research*, *115*, A11222. https://doi.org/10.1029/2010JA015707

Fu, H. S., Cao, J. B., Zhima, Z., Khotyaintsev, Y. V., Angelopoulos, V., Santolik, O., et al. (2014). First observation of rising-tone magnetosonic waves. *Geophysical Research Letters*, *41*, 7419–7426. https://doi.org/10.1002/2014GL061867

Gary, S. P., Liu, K., Winske, D., & Denton, R. E. (2010). Ion Bernstein instability in the terrestrial magnetosphere: Linear dispersion theory. *Journal of Geophysical Research*, *115*, A12209. https://doi.org/10.1029/2010JA015965

Gurnett, D. A. (1976). Plasma wave interactions with energetic ions near the magnetic equator. *Journal of Geophysical Research*, *81*, 2765–2770. https://doi.org/10.1029/JA081i016p02765

Horne, R. B., & Thorne, R. M. (1998). Potential waves for relativistic electron scattering and stochastic acceleration during magnetic storms. *Geophysical Research Letters*, *25*(15), 3011–3014.

Horne, R. B., Thorne, R. M., Glauert, S. A., Albert, J. M., Meredith, N. P., & Anderson, R. R. (2005). Timescale for radiation belt electron acceleration by whistler mode chorus waves. *Journal of Geophysical Research*, *110*, A03225. https://doi.org/10.1029/2004JA010811

Horne, R. B., Thorne, R. M., Glauert, S. A., Meredith, N. P., Pokhotelov, D., & Santolik, O. (2007). Electron acceleration in the Van Allen radiation belts by fast magnetosonic waves. *Geophysical Research Letters*, *34*, L17107. https://doi.org/10.1029/2007GL030267

Lei, M., Xie, L., Li, J., Pu, Z., Fu, S., Ni, B., et al. (2017). The radiation belt electron scattering by magnetosonic wave: Dependence on key parameters. *Journal of Geophysical Research: Space Physics*, *122*, 12,338–12,352. https://doi.org/10.1002/2016JA023801

Li, J., Ni, B., Xie, L., Pu, Z., Bortnik, J., Thorne, R. M., et al. (2014). Interactions between magnetosonic waves and radiation belt electrons: Comparisons of quasi-linear calculations with test particle simulations. *Geophysical Research Letters*, *41*, 4828–4834. https://doi.org/10.1002/2014GL060461

Liu, K. J., Gary, S. P., & Winske, D. (2011). Excitation of magnetosonic waves in the terrestrial magnetosphere: Particle-in-cell simulations. *Journal of Geophysical Research*, *116*, A07212. https://doi.org/10.1029/2010JA016372

Ma, Q. L., Li, W., Thorne, R. M., & Angelopoulos, V. (2013). Global distribution of equatorial magnetosonic waves observed by THEMIS. *Geophysical Research Letters*, *40*, 1895–1901. https://doi.org/10.1002/grl.50434

Means, J. D. (1972). Use of the three-dimensional covariance matrix in analyzing the polarization properties of plane waves. *Journal of Geophysical Research*, *77*(28), 5551–5559. https://doi.org/10.1029/JA077i028p05551

Meredith, N. P., Horne, R. B., & Anderson, R. R. (2008). Survey of magnetosonic waves and proton ring distributions in the Earth's inner magnetosphere. *Journal of Geophysical Research*, *113*, A06213. https://doi.org/10.1029/2007JA012975

Min, K., & Liu, K. (2016). Proton velocity ring-driven instabilities in the inner magnetosphere: Linear theory and particle-in-cell simulations. *Journal of Geophysical Research: Space Physics*, *121*, 475–491. https://doi.org/10.1002/2015JA022042

Mourenas, D., Artemyev, A. V., Agapitov, O. V., & Krasnoselskikh, V. (2013). Analytical estimates of electron quasilinear diffusion by fast magnetosonic waves. *Journal of Geophysical Research: Space Physics*, *118*, 3096–3112. https://doi.org/10.1002/jgra.50349

Ni, B. B., Hua, M., Zhou, R. X., Yi, J., & Fu, S. (2017). Competition between outer zone electron scattering by plasmaspheric hiss and magnetosonic waves. *Geophysical Research Letters*, *44*, 3465–3474. https://doi.org/10.1002/2017GL072989

Perraut, S., Roux, A., Robert, P., Gendrin, R., Sauvaud, J., Bosqued, J., et al. (1982). A systematic study of ULF waves above F/H+ from GEOS 1 and 2 measurements and their relationships with proton ring distributions. *Journal of Geophysical Research*, *87*, 6219–6236. https://doi.org/10.1029/JA087iA08p06219

Russell, C. T., Holzer, R. E., & Smith, E. J. (1970). OGO 3 observations of ELF noise in the magnetosphere: 2. The nature of the equatorial noise. *Journal of Geophysical Research*, *75*(4), 755–768. https://doi.org/10.1029/JA075i004p00755

Santolík, O., Pickett, J. S., Gurnett, D. A., Maksimovic, M., & Cornilleau-Wehrlin, N. (2002). Spatiotemporal variability and propagation of equatorial noise observed by cluster. *Journal of Geophysical Research*, *107*(A12), 1495. https://doi.org/10.1029/2001JA009159

Sun, J., Gao, X., Chen, L., Lu, Q., Tao, X., & Wang, S. (2016). A parametric study for the generation of ion Bernstein modes from a discrete spectrum to a continuous one in the inner magnetosphere. I. Linear theory. *Physics of Plasmas*, *23*(2), 022901. https://doi.org/10.1063/1.4941283

Sun, J., Gao, X., Ke, Y., Lu, Q., Wang, X., & Wang, S. (2019). Expansion of solar coronal hot electrons in an inhomogeneous magnetic field: 1-D PIC simulation. *The Astrophysical Journal*, *887*, 96. https://doi.org/10.3847/1538-4357/ab5060

Sun, J., Gao, X., Lu, Q., Chen, L., Liu, X., Wang, X., et al. (2017). Spectral properties and associated plasma energization by magnetosonic waves in the Earth's magnetosphere: Particle-in-cell simulations. *Journal of Geophysical Research: Space Physics*, *122*, 5377–5390. https://doi.org/10.1002/2017JA024027

Sun, J., Gao, X., Lu, Q., Chen, L., Tao, X., & Wang, S. (2016). A parametric study for the generation of ion Bernstein modes from a discrete spectrum to a continuous one in the inner magnetosphere. II. Particle-in-cell simulations. *Physics of Plasmas*, *23*(2), 022902. https://doi.org/10.1063/1.4941284

Tao, X., & Li, X. (2016). Theoretical bounce resonance diffusion coefficient for waves generated near the equatorial plane. *Geophysical Research Letters*, *43*, 7389–7397. https://doi.org/10.1002/2016GL070139

Tsurutani, B. T., Falkowski, B. J., Pickett, J. S., Verkhoglyadova, O. P., Santolik, O., & Lakhina, G. S. (2014). Extremely intense ELF magnetosonic waves: A survey of polar observations. *Journal of Geophysical Research: Space Physics*, *119*, 964–977. https://doi.org/10.1002/2013JA019284

Xiao, F. L., Yang, C., Su, Z. P., Zhou, Q. H., He, Z. G., He, Y. H., et al. (2015). Wave-driven butterfly distribution of Van Allen belt relativistic electrons. *Nature Communications*, *6*(1), 8590. https://doi.org/10.1038/ncomms9590

Yuan, Z., Yao, F., Yu, X., Huang, S., & Ouyang, Z. (2019). An automatic detection algorithm applied to fast magnetosonic waves with observations of the Van Allen probes. *Journal of Geophysical Research: Space Physics*, *124*, 3501–3511. https://doi.org/10.1029/2018JA026387

Yuan, Z., Yu, X., Huang, S., Qiao, Z., Yao, F., & Funsten, H. O. (2018). Cold ion heating by magnetosonic waves in a density cavity of the plasmasphere. *Journal of Geophysical Research: Space Physics*, *123*, 1242–1250. https://doi.org/10.1002/2017JA024919

Zou, Z., Zuo, P., Ni, B., Wei, F., Zhao, Z., Cao, X., et al. (2019). Wave normal angle distribution of fast magnetosonic waves: A survey of Van Allen probes EMFISIS observations. *Journal of Geophysical Research: Space Physics*, *124*, 5663–5674. https://doi.org/10.1029/2019JA026556